Applied Nanoscience (2020) 10:1481–1488
https://doi.org/10.1007/s13204-020-01266-5

ORIGINAL ARTICLE

Facile synthesis and properties of chromium-doped cobalt oxide (Cr-doped Co_3O_4) nanostructures for supercapacitor applications

Faisal Ali[1] · **N. R. Khalid**[1]

Received: 15 October 2019 / Accepted: 23 January 2020 / Published online: 11 February 2020

Abstract

Chromium-doped cobalt oxide (Cr_x-doped Co_3O_4 $x = 1$–10 at%) nanoflowers were synthesized by a facile hydrothermal method. The structure, morphology, composition, and optical properties were analyzed with X-ray powder diffraction, scanning electron microscopy, energy-dispersive X-ray, and photoluminescence spectroscopy. The electrochemical properties of the chromium-doped cobalt oxide (Cr_x-doped Co_3O_4 $x = 1$–10 at%) nanoflowers were measured by cyclic voltammetry, galvanostatic charge–discharge, and electrochemical impedance spectroscopy in 3 M KOH electrolyte. The 6 at% Cr-doped Co_3O_4 sample has demonstrated 1283 Fg^{-1} specific capacitance at 5 mV/s scan rate which is 67% more than pristine Co_3O_4 having specific capacitance 860.56 Fg^{-1}. Moreover, it has presented outstanding specific capacitance retention of 72.86% after 1000 continuous charge–discharge cycles. These excellent electrochemical properties of 6 at% chromium-doped cobalt oxide (Cr_x-doped Co_3O_4 $x = 6$ at%) nanoflowers showed that it is promising material for supercapacitor applications.

Keywords Cr_x-doped Co_3O_4 (where $x = 1$–10 at%) · Nanoflowers · Hydrothermal synthesis method · Electrochemical properties

Introduction

The demand of renewable energy sources has been increased during recent years due to increasing population, and thus, researchers have great responsibility to find out some sophisticated energy storing devices to overcome the shortage of renewable energy sources (Zuo et al. 2017). Among this, energy storing device such as the supercapacitor is more famous due to its outstanding characteristics including fast charging–discharging rate, efficient power density, outstanding cyclic performance, and excellent charge retention. The supercapacitor consists of two major types such as EDL that is electric double layer which operates on non-faradic charge–discharge principle and the second is pseudo capacitor which operates on faradic oxidation–reduction reactions (Wang 2017). The electrochemical performance of the supercapacitor's electrode is majorly important for highly efficient device. Therefore, for this purpose, a lot of materials have been used such as transition metal oxide, conducting polymers, carbon-based materials, etc. Among these, transition metal oxides were majorly used due to multiple oxidation states of transition metals and high capacitance values (Zhao 2015). It is well known that RuO_2 has been proved as one of the best electrode materials, because it showed excellent capacitive performance. However, its high cost is one of the major problems; therefore, it is not good choice for commercial scale use (Qiu 2014; Kazemi and Asghari 2014).

On the other hand, the cobalt oxide (Co_3O_4) is considered one of the best choices as electrode material for supercapacitor applications owing to its higher theoretical capacitance, i.e., 3560 F/g (Cheng 2010). Along with high theoretical capacitance, cobalt oxide has also excellent characteristics including low cost, efficient in reversible redox reactions, environment friendly, nontoxicity, multiple morphologies like nanocubes, nanorods, and nanospheres, etc. (Kwak et al. 2013). Besides these excellent properties of cobalt oxide experimentally, it is not possible to obtain higher capacitance values of cobalt oxide matching with its theoretical value due to some technical reasons. However, by adopting some novel techniques, its capacitance, energy density, and other electrochemical characteristics can be enhanced. Among them, morphological modification of cobalt oxide is good approach to

✉ N. R. Khalid
khalid.nadeem@uog.edu.pk

[1] Department of Physics, Faculty of Sciences, University of Gujrat, Hafiz Hayat Campus, Gujrat 50700, Pakistan

enhance the efficiency as electrode material. Previously, researchers have synthesized various morphologies including nanoneedles, nanospheres, nanocages, nanocubes, nanorods, nanotubes, nanofibers, nanolayered, and nanoparticles which have greater influence on electrochemical characteristics of cobalt oxide (Zhang 2012; Xiao 2014; Xu 2010; Zhang and Zou 2013; Kumar et al. 2014; Duan and Cao 2012; Deng 2014). However, the cobalt oxide nanostructures have low conductivity which results in low ionic kinetics and low specific capacitance than theoretical value. To improve this characteristic, different researchers have synthesized cobalt oxide-based composites using conducting polymers, metal oxides, and carbon, but none of these have proved as fundamental solution to enhance its electrochemical properties (Salunkhe 2015; Wu 2017; Tang et al. 2013; Li 2019). Therefore, different researchers have tried to optimize its electrochemical properties via doping with different transition metal ions and it was found effective to improve its efficiency for supercapacitor (Wang et al. 2018; Patil 2011; Zhu 2018).

Guangmin Li et al. have reported that manganese doping into Co_3O_4 mesoporous nanoneedles have enhanced specific capacitance from 201.3 F/g of pure cobalt oxide to 668.4 F/g along with an ultra-cyclic stability of 104% after 10,000 cycles of charging–discharging (Li 2019). Similarly 5% cadmium doping into Co_3O_4 nanosheets has improved capacitance equal to 737 Fg^{-1} which was 69% higher as compare to pure cobalt oxide (Deng 2016). Moreover, it was found in the literature that chromium doping into cobalt oxide (Co_3O_4) is also very effective to enhance its efficiency in catalysis and gas-sensing applications due to excellent properties of chromium metal (Priyadharshini 2018; Kharade 2018; Zhou 2018). However, to the best of our knowledge, chromium-doped cobalt oxide (Cr-doped Co_3O_4) has not been reported for electrochemical supercapacitor applications.

In this work, we have synthesized chromium-doped cobalt oxide (Cr-doped Co_3O_4) nanoflowers as electrode material for supercapacitor first time using a facile hydrothermal method. Furthermore, XRD, SEM, EDX, and PL spectroscopy were used for the characterization of synthesized nanostructures. The electrochemical properties of all samples were measured using CV, GCD, and EIS techniques.

Experimental section

Chemical reagents

Cobalt chloride ($CoCl_2$), chromium chloride ($CrCl_2$), polyvinylpyrrolidone (PVP), urea (NH_2CONH_2), and ethanol (C_2H_5OH) were bought from Sigma-Aldrich and used without any additional refinement.

Synthesis of Cr-doped Co_3O_4 nanostructures

For the synthesis of Cr-doped Co_3O_4, first solution was prepared by dissolving 24.9 mmol of $CoCl_2$ into 20 mL deionized H_2O. Second, 0.5 mmol $CrCl_2$ was separately dissolved in 10 mL of deionized water (DI H_2O). Then, the second solution was dropwise added into the first solution of $CoCl_2$ via burette under continuous stirring of 1 h. After that, NaOH solution of 55 mmol was added to above solution to maintain neutral pH of the solution. In the next step, 1.5 g PVP and 1.5 g urea were also added as a surfactant in the above solution. For hydrothermal treatment, final solution transferred into a Teflon lined (TL) autoclave of 100 mL volume capacity and placed for 12 h heating at 180 C temperature in an oven. After this, the obtained final product was cool down and washed by ethanol and deionized water for six times to obtain neutral pH of 7 and dried at 80 °C for 10 h. In the last step, the obtained material was calcined at 550 °C for 2 h in a muffle furnace. The chromium-doping ratio into cobalt oxide was varied from 1 to 10 at% and labelled as 2Cr–Co_3O_4, 4Cr–Co_3O_4, 6Cr–Co_3O_4, 8Cr–Co_3O_4, and 10Cr–Co_3O_4. The pristine cobalt oxide was also prepared using the same procedure without adding chromium source.

Fabrication of electrode and electrochemical testing

A three-electrode system was employed to test the electrochemical performance of chromium-doped cobalt oxide nanostructures. In this system, the platinum foil suspended in 3 M KOH electrolyte solution was used as counter electrode and Ag/AgCl was reference electrode. Moreover, the working electrode was made from chromium-doped cobalt oxide nanostructure. Typically, the working electrode was fabricated through mixing of 80 wt% Cr-doped Co_3O_4 material, 10 wt% activated carbon, and 10 wt% polyvinylidene fluoride with ethanol. Then, formed homogeneous slurry was coated onto a 1 cm^2 nickel foam and dried at 110 °C.

For electrochemical testing of prepared samples, the Gamry 5000 interface workstation was used in this study. The electrochemical properties were observed by galvanostatic charge–discharge and cyclic voltammetry (CV) techniques. Electrochemical impedance spectroscopy (EIS) measurements were performed in the frequency range of 1 Hz–10 kHz.

Characterization of Cr-doped Co_3O_4 nanostructures

The crystal structure of Cr-doped Co_3O_4 nanostructures was investigated by X-ray powder diffraction (XRD, Rigaku, Cu Kα, $\lambda = 1.5418$ A°). The scanning electron microscopy (LEO

1450 VP, SEM) was employed to examine the morphology and elemental composition of prepared sample. The optical properties of prepared materials were determined using photoluminescence (PL) spectroscopy (JASCO, FP-8200).

Results and discussion

XRD analysis

The crystalline structure of the pristine Co_3O_4 and Cr-doped Co_3O_4 nanostructures was examined by XRD and results are shown in Fig. 1a, b. The pure cobalt oxide has exhibited the cubic phase of Co_3O_4 according to JCPDS No. 01-076-1802. Interestingly, all doped cobalt oxide samples also displayed same cubic phase of Co_3O_4 nanostructure without any impurity. It can be seen from results that there is no obvious change in the diffraction patterns of doped samples; only a little shift towards lower 2Θ angle was observed. This clearly confirms that Cr has been successfully incorporated into the structure of Co_3O_4. Moreover, the crystallite size of all samples was determined using Debye Scherer's equation. The calculated average crystallite sizes were 10.2 nm, 9.6 nm, 9.1 nm, 8.5 nm, 8.9 nm, and 9.3 nm for pure Co_3O_4, $2Cr–Co_3O_4$, $4Cr–Co_3O_4$, $6Cr–Co_3O_4$, $8Cr–Co_3O_4$, and $10Cr–Co_3O_4$ samples, respectively. This shows that crystallite size was decreased up to 6 at% Cr doping; however, further increase in Cr doping ratio had negative influence on crystallite size of sample. This decrease in crystallite size might be attributed to little ionic radii difference of Co^{3+} (69 pm) and Cr^{3+} (76 pm) as previously reported (Wang 2011).

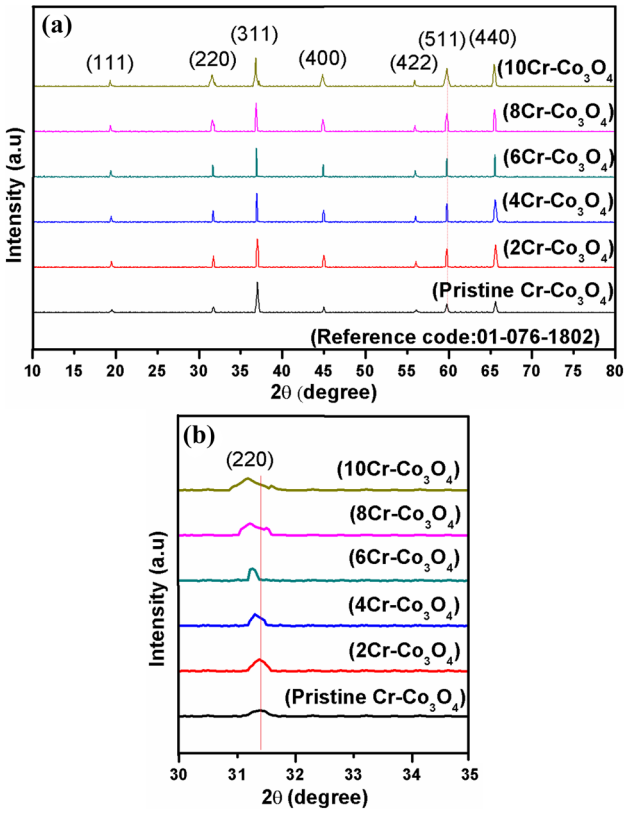

Fig. 1 **a** X-ray diffraction patterns of pristine and 2-10Cr–Co_3O_4 nanostructures and (**b**) magnified version of (311) plane

SEM/EDX analysis

The morphology of $6Cr–Co_3O_4$ sample was examined by employing SEM and images are shown in the Fig. 2a, b. It can be seen that the $6Cr–Co_3O_4$ sample displayed nanoflower like morphology. The diameter of nanoflowers is about 200 nm, while width of petals is in the range of 20–50 nm confirming formation of nanostructures. This development of nanoflowers like morphology of $6Cr–Co_3O_4$ may offer additional active sites for electrochemical reactions due to higher surface area of nanostructure. Moreover, there might be more efficient contact between electrolyte ions and surface of electrode material which can enhance its capacitive ability.

The elemental composition of $6Cr–Co_3O_4$ was determined using EDX and result is shown in Fig. 2c. The atomic percentage of the elements present in $6Cr–Co_3O_4$ has been displayed in the table (inset of Fig. 2c). These ratios verify that the cobalt and oxygen are near to stoichiometric which is in agreement with 3:4 ratios of cobalt and oxygen in Co_3O_4. Furthermore, the 5.09 at% Cr ratio also confirms the presence of Cr in $6Cr–Co_3O_4$ sample which is approximately equal to 6 at. % doping ratio of Cr in Co_3O_4 nanostructure.

Capacitive studies

Cyclic voltammetric studies

The capacitive/electrochemical characteristics of pristine Co_3O_4 and Cr-doped Co_3O_4 nanostructures were tested by the cyclic voltammetry technique at 5 mVs^{-1} scan rate in the potential window −0.1 to +0.75 V, and results are displayed in Fig. 3a. The specific capacitance of all samples was calculated using data of Fig. 3a by the following equation (Wang 2011):

$$C = \int \frac{I\mathrm{d}t}{mv\Delta V}, \tag{1}$$

where "I" denotes the oxidation/reduction current, "dt" represents the time differential, "m" denotes active electrode material's mass, and "ΔV" is the range of voltage for one sweep segment. The calculated specific capacitance values are 860.56 Fg^{-1}, 931.78 Fg^{-1}, 952.28 Fg^{-1},

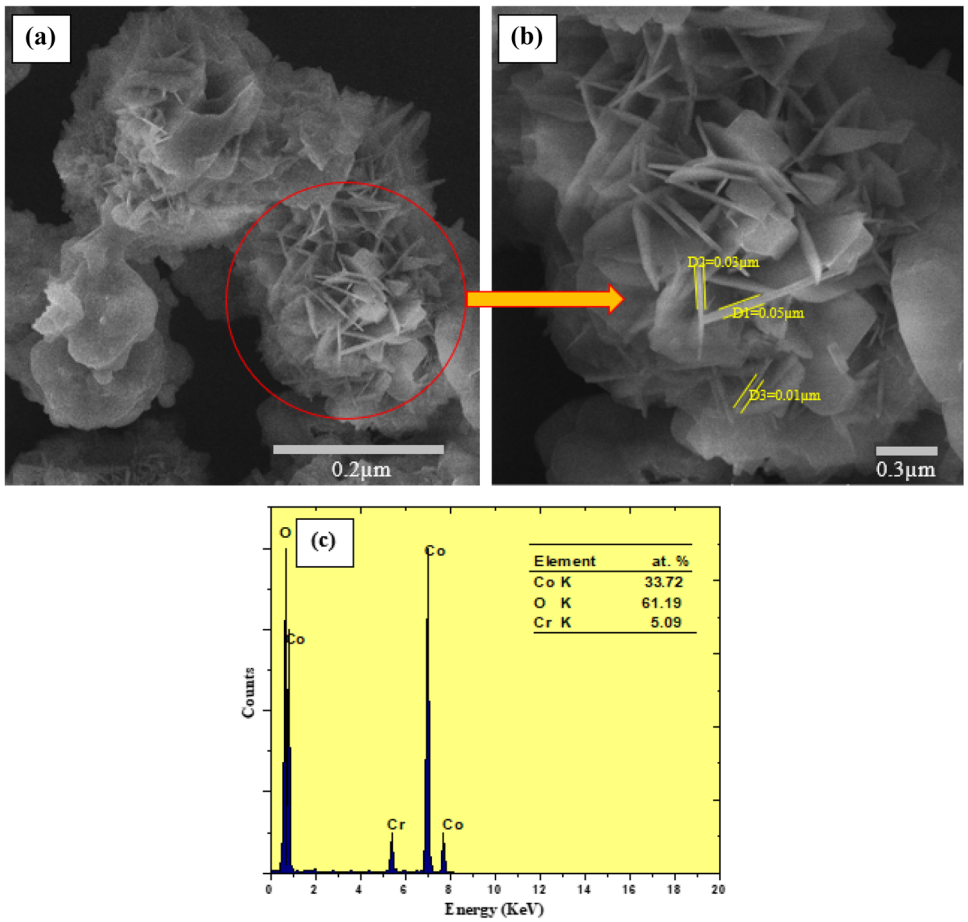

Fig. 2 **a** SEM micrograph of 6Cr–Co_3O_4, (**b**) magnified micrograph of 6Cr–Co_3O_4, and (**c**) EDS spectrum of 6Cr-Co_3O_4

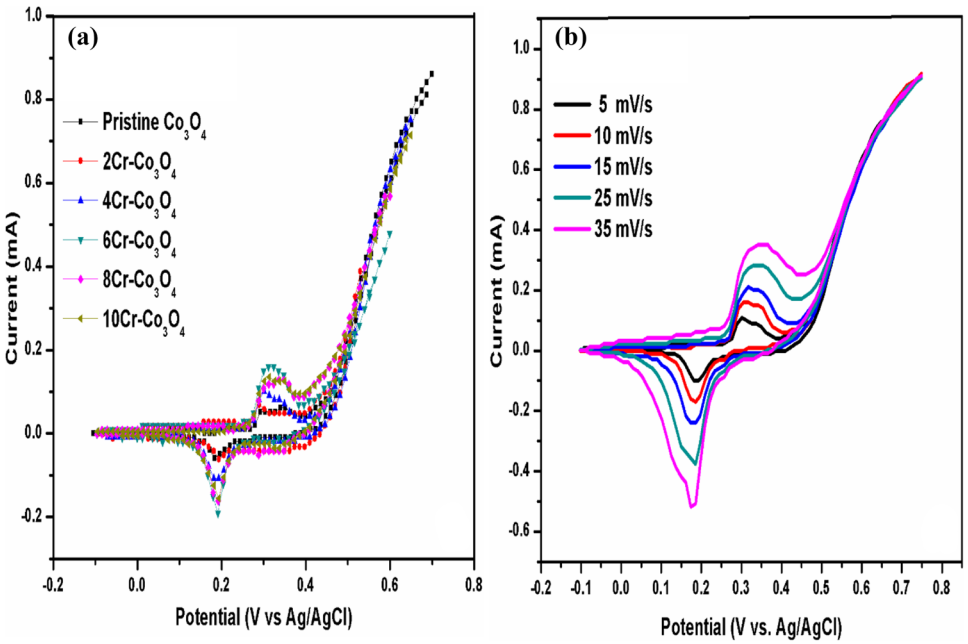

Fig. 3 a CV curves of pristine and 2-10Cr-Co_3O_4 nanostructures at 5 mV-1 scan rate, respectively, and **b** CV curves of 6Cr–Co_3O_4 nanostructures at different scan rates, respectively

1283.06 Fg^{-1}, 1029.59 Fg^{-1}, and 941.52 Fg^{-1} for pristine Co_3O_4, 2Cr–Co_3O_4, 4Cr–Co3O4, 6Cr–Co_3O_4, 8Cr–Co_3O_4, and 10Cr–Co_3O_4 respectively. Among all samples, the 6Cr–Co_3O_4 has showed highest specific capacitance value of 1283.06 Fg^{-1} which is 67% more than pristine Co_3O_4. Interestingly, this value of specific capacitance is also higher than previously reported values in the literature, as shown in Table 1. It could be attributed to the optimum doping level of chromium metal into Co_3O_4 nanostructure. Furthermore, this specific capacitance enhancement could be ascribed to the formation of nanoflowers which has higher active surface area, thus providing excessive active sited for faradaic redox reactions. Second, the decrease in specific capacitance value of Cr-doped Co_3O_4 nanostructure above 6% Cr doping might be due to excessive doping of Cr which has covered the surface of electrode material and decreased the surface-active sites. The cyclic voltammetric results of 6Cr–Co_3O_4 at 5 mVs^{-1}, 10 mVs^{-1}, 15 mVs^{-1}, 25 mVs^{-1}, and 35 mVs^{-1} scan rates are shown in Fig. 3(b). The results demonstrate that 6Cr–Co_3O_4 sample has showed typical pseudocapacitive characteristics having a pair of redox peaks which confirms the conversion of Co_3O_4 into CoO_2 as displayed in Eq. 2 (Qiu 2015):

$$Co_3O_4 + 4OH^- \leftrightarrow 3CoO_2 + 4e^- + 2H_2O. \quad (2)$$

To understand the specific capacitance enhancement, a mechanism for 6Cr-doped Co_3O_4 nanostructure-based supercapacitor is shown in Fig. 4a–c. The nanoflower-based structure of 6Cr–Co_3O_4 having defects produced due to doping of Cr in Co_3O_4 nanostructure is presented in Fig. 4a. The redox reactions occurred at the working electrode surface for undoped and doped nanostructures of Co_3O_4 are shown, respectively, in Fig. 4b. It is proposed that the doping of Cr ions into Co_3O_4 crystal lattice has stopped particle agglomeration resulting in the formation of flower like nanostructures which created additional active sites for more faradaic redox reactions due to defects in the petals of flower nanostructures. Furthermore, the calcination of the material at 550 °C has also produced additional oxygen vacancies. Therefore, these factors have improved the conduction path of charges and thus facilitated the charges kinetics resulting in high conductivities. Moreover, in addition to Co_3O_4, the doped Cr ions into Co_3O_4 has also participated in faradaic redox reactions of Cr^{4+}/Cr^{3+} and the possible reaction (Fig. 4c) is given in Eqs. 3 and 4 (Cummings 2012):

$$CrO(OH) + OH^- \leftrightarrow CrO(OH)_2 + e^- \quad (3)$$

$$CrO(OH)_2 + OH^- \leftrightarrow CrO(OH)_3 + e^-. \quad (4)$$

Thus, 6Cr–Co_3O_4 nanostructure has displayed enhanced performance. The cyclic performance of 6Cr–Co_3O_4 has been also tested for 1000 cycles and results are presented in Fig. 5. This sample showed good cyclic performance and the capacitance retention after 1000 CV cycles was found about 72.86%.

Table 1 Comparison of specific capacitance values for various pristine and doped Co_3O_4 nanostructures

Material	Specific capacitance (F/g)	Scan rate (mV/s)	Electrolyte	Synthesis method	References
Co_3O_4 nanopowders	291	10	2 M KOH	Chemical reduction	Priyadharshini (2018)
Hydrophilic Co_3O_4	315	5	0.5 M Na_2SO_4	Galvanostatic electrodeposition	Kharade (2018)
Co_3O_4 nanofibers	407	5	6 M KOH	Electrospinning	Kumar et al. (2014)
0.4Sn doped Co_3O_4 nanowires	151.8	5	6 M KOH	Hydrothermal	Zhou (2018)
3% B-doped Co_3O_4 thin films	482.35	5	6 M KOH	Spray deposition	Kerli (2016)
Manganese-doped Co_3O_4 mesoporous nanoneedles	668.4	1 A/g	2 M KOH	Hydrothermal	Li (2019)
1% Mn-doped Co_3O_4 thin film	675	10	0.1 M KOH	Sol–gel spin coat deposition	Jogade and Sutrave (2017)
Mn-doped Co_3O_4	773	1 A/g	2 M KOH	Solvothermal	Chen (2019a)
Mn-doped Co_3O_4 oblique prisms	909	1 A/g	2 M KOH	Solvothermal reaction	Chen (2019b)
Co_3O_4 nanosheets	436	1 A/g	6 M KOH	Chemical coprecipitation	Deng (2016)
Co_3O_4 nanosheets Cd 5%	737				
Co_3O_4 nanostructures	860.56	5	3 M KOH	Hydrothermal	This work
6Cr–Co_3O_4	1283.06				

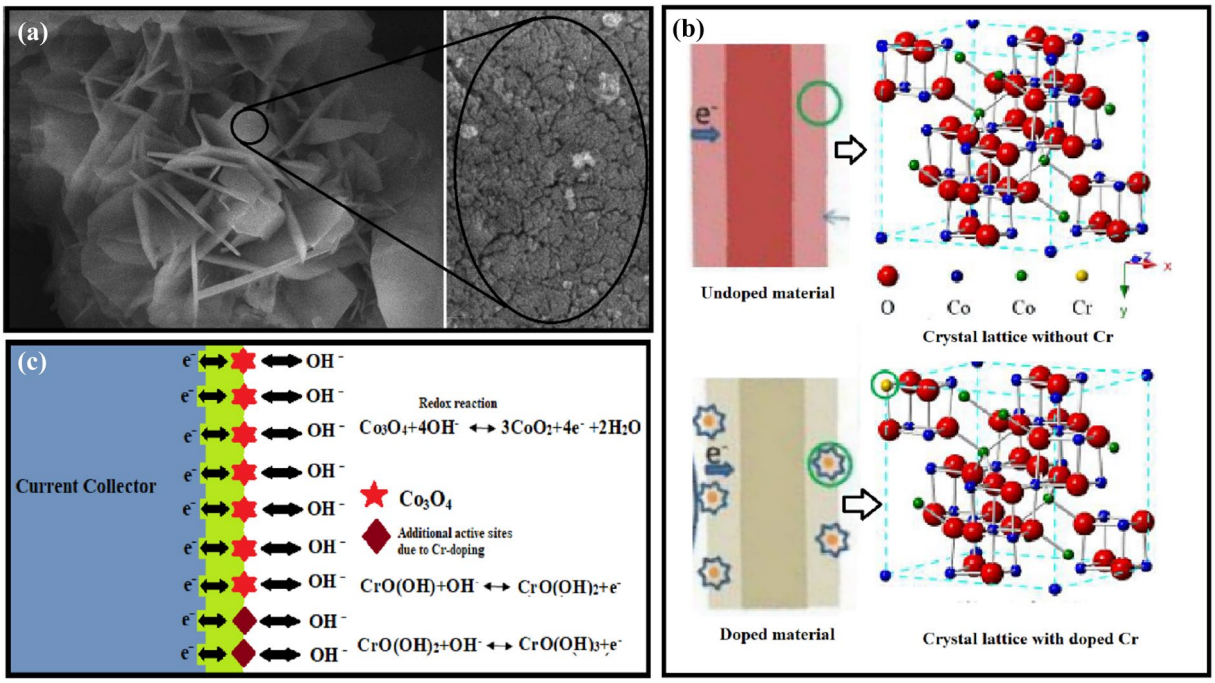

Fig. 4 **a**–**c** Capacitance enhancement mechanism due to doping of Cr in Co_3O_4 nanostructures

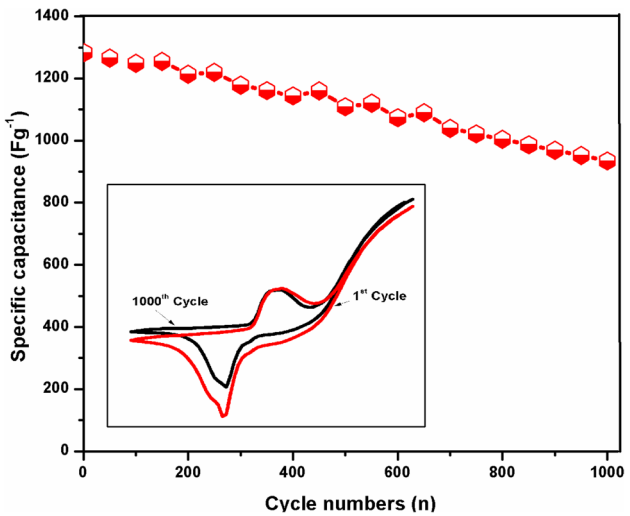

Fig. 5 The cyclic performance of 6Cr–Co_3O_4

Charge–discharge studies

The GCD curves of 6Cr–Co_3O_4 at 1 Ag^{-1}, 2 Ag^{-1}, 4 Ag^{-1}, 6 Ag^{-1}, and 10 Ag^{-1} current densities are shown in Fig. 6a. The small additional convexer in the results is due to chromium doping which participated in the redox reactions. Furthermore, the non-linear behavior of the voltage plateau has confirmed the pseudocapacitive nature of as-prepared nanostructures, because electrochemical reactions occur due to redox mechanisms at electrode material. It can be observed that there is a minor voltage drop during discharging indicating high conductive nature of these nanostructures. Furthermore, the discharge time was decreased as current densities increased from 1 to 10 Ag^{-1}. Second, the specific capacitances values were also decreased from 1271.39 to 1264.10 Fg^{-1}, 1249.57 Fg^{-1}, 1235.04 Fg^{-1}, and 1204.08 Fg^{-1} as current densities increased from 1 to 10 Ag^{-1}, respectively. It could be attributed to less ion diffusion in electrolyte and charge transfer in the electrode material resulting in less active material's participation in redox reactions and thus increase in the polarization value at higher current densities.

Electrochemical impedance studies

This technique is also used to test the capacitive characteristic of the electrode material. In general, its Nyquist plot consists of two sections: first section consists of an arc and occurs in the range of high frequency and other section represents an inclined line in the low-frequency range. The inherent resistance of the material of electrode, resistance of electrolyte, and the resistance due to the interaction between working electrode and collector are indicated by "Rs" which can be obtained by intersection point in the high-frequency range. The diffusion resistance can be obtained by linear line in the low-frequency range. More the vertical nature of the linear line, less will be the diffusion resistance. The Nyquist plots are shown in Fig. 6b. The value of "Rs" has decreased up to 6% Cr doping into Co_3O_4 and this sample has exhibited

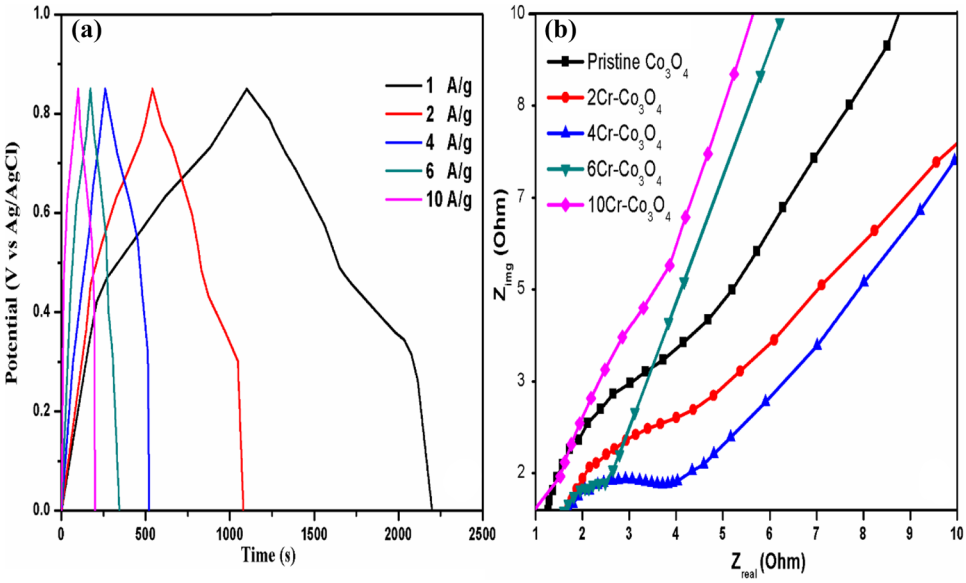

Fig. 6 **a** Galvanostatic charging–discharging (GCD) curves of 6Cr–Co_3O_4 at 1 A/g, 2 A/g, 4 A/g, 6 A/g, and 10 A/g current densities and (**b**) electrochemical impedance spectroscopy (EIS) curves of pristine and 2-10Cr–Co_3O_4 nanostructures

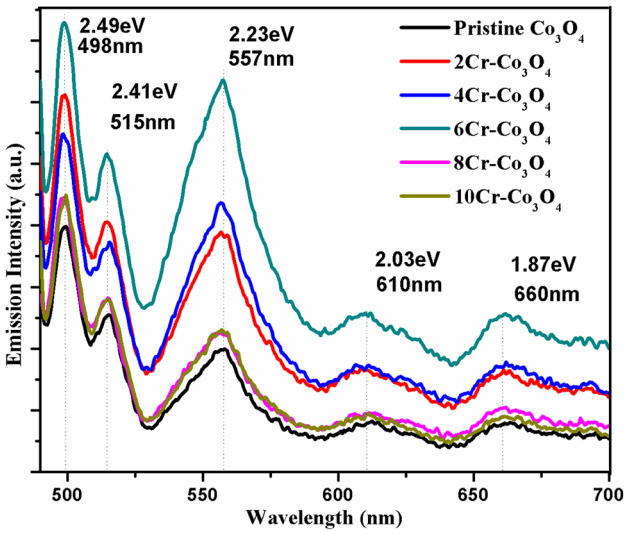

Fig. 7 Room temperature PL spectra of pristine and 2-10Cr–Co_3O_4 nanostructures

minimum "Rs" value. Therefore, as a result, this sample will be more conductive as was seen in CV results where this sample has exhibited maximum specific capacitance. Similarly, "Rct" resistance has also been decreased up to 6% Cr doping into Co_3O_4, because its semicircle's diameter is minimum as compared to pristine Co_3O_4 and other doped sample showing good charges kinetics.

Photoluminescence studies

It is a sophisticated method to study defects of both types extrinsic and intrinsic in semiconductor-based materials (Tarwal 2014). This technique is very helpful to investigate the crystal quality of nanostructure materials. The measured photoluminescence spectra at room temperature of pristine and Cr-doped Co_3O_4 are displayed in Fig. 7. At excitation wavelength of 480 nm, there is most intense emission peak at 557 nm (green light) along with two less intense emission peaks at 610 nm (red light) and 660 nm (red light). According to some reports at 557 nm wavelength, the green emission band appears due to holes recombination with electrons existed in separately ionized oxygen positions (V^+O) (Vanheusden 1996). Intensity of green light's emission peak has been increased with the addition of chromium up to 6% Cr doping into Co_3O_4 showing the increase in oxygen vacancies in Co_3O_4 due to doping of Cr^{3+}. However, further increase in Cr doping into Co_3O_4 has decreased the PL emission intensity which confirms the coverage of surface-active sites.

Conclusions

In summary, the pristine and Cr-doped Co_3O_4 nanoflowers were prepared by a facile hydrothermal technique. The 6 at% Cr-doped Co_3O_4 has exhibited a high specific capacitance equal to 1283 Fg^{-1} at scan rate 5 mVs^{-1} which is 67% more than pristine Co_3O_4 having specific capacitance equal to 860.56 Fg^{-1}. The prepared novel electrode nanostructure showed that excellent cycling stability and cyclic retention of 72.86% was observed after 1000 cycles. Moreover, the photoluminescence spectroscopy has showed the most intense emission peak at 557 nm which represents the green light emission of Cr-doped cobalt oxide nanostructures. The excellent capacitive properties of 6 at% Cr-doped Co_3O_4 nanostructures prove that it has high capability to be used as electrode material for supercapacitor application.

References

Chen H et al (2019a) Uniform and porous Mn-doped Co3O4 microspheres: solvothermal synthesis and their superior supercapacitor performances. Ceram Int 45(9):11876–11882

Chen H et al (2019b) Facile synthesis of porous Mn-doped Co3O4 oblique prisms as an electrode material with remarkable pseudocapacitance. Ceram Int 45(6):8008–8016

Cheng H et al (2010) A facile method to improve the high rate capability of Co_3O_4 nanowire array electrodes. Nano Research 3(12):895–901

Cummings CY et al (2012) Surface state trapping and mobility revealed by junction electrochemistry of Nano-Cr_2O_3. Aust J Chem 65(1):65–71

Deng J et al (2014) Solution combustion synthesis of cobalt oxides (Co_3O_4 and Co_3O_4/CoO) nanoparticles as supercapacitor electrode materials. Electrochim Acta 132:127–135

Deng S et al (2016) Cd doped porous Co_3O_4 nanosheets as electrode material for high performance supercapacitor application. Electrochim Acta 196:316–327

Duan B, Cao Q (2012) Hierarchically porous Co_3O_4 film prepared by hydrothermal synthesis method based on colloidal crystal template for supercapacitor application. Electrochim Acta 64:154–161

Jogade S, Sutrave D (2017) Electrochemical performance of Mn doped Co_3O_4 supercapacitor: effect of aqueous electrolytes. J Mater Sci Eng 6:351

Kazemi S, Asghari A (2014) High performance supercapacitors based on the electrodeposited Co_3O_4 nanoflakes on electro-etched carbon fibers. Electrochim Acta 138:9–14

Kerli S (2016) Boron-doped cobalt oxide thin films and its electrochemical properties. Mod Phys Lett B 30(27):1650343

Kharade P et al (2018) Electrodeposited nanoflakes like hydrophilic Co_3O_4 as a supercapacitor electrode. J Phys Chem Solids 120:207–210

Kumar M, Subramania A, Balakrishnan K (2014) Preparation of electrospun Co_3O_4 nanofibers as electrode material for high performance asymmetric supercapacitors. Electrochim Acta 149:152–158

Kwak JH, Lee Y-W, Bang JH (2013) Supercapacitor electrode with an ultrahigh Co_3O_4 loading for a high areal capacitance. Mater Lett 110:237–240

Li G et al (2019) Manganese doped Co_3O_4 mesoporous nanoneedle array for long cycle-stable supercapacitors. Appl Surf Sci 469:941–950

Patil D et al (2011) An Mn doped polyaniline electrode for electrochemical supercapacitor. J Electrochem Soc 158(6):A653–A657

Priyadharshini T et al (2018) Hexamine role on pseudocapacitive behaviour of cobalt oxide (Co_3O_4) nanopowders. J Nanosci Nanotechnol 18(6):4093–4099

Qiu K et al (2014) Hierarchical 3D mesoporous conch-like Co_3O_4 nanostructure arrays for high-performance supercapacitors. Electrochim Acta 141:248–254

Qiu K et al (2015) Ultrathin mesoporous Co_3O_4 nanosheets on Ni foam for high-performance supercapacitors. Electrochim Acta 157:62–68

Salunkhe RR et al (2015) Asymmetric supercapacitors using 3D nanoporous carbon and cobalt oxide electrodes synthesized from a single metal–organic framework. ACS Nano 9(6):6288–6296

Tang C-H, Yin X, Gong H (2013) Superior performance asymmetric supercapacitors based on a directly grown commercial mass 3D Co_3O_4@Ni (OH) 2 core–shell electrode. ACS Appl Mater Interfaces 5(21):10574–10582

Tarwal N et al (2014) Structure, X-ray photoelectron spectroscopy and photoluminescence investigations of the spray deposited cobalt doped ZnO thin films. J Anal Appl Pyrol 106:26–32

Vanheusden K et al (1996) Mechanisms behind green photoluminescence in ZnO phosphor powders. J Appl Phys 79(10):7983–7990

Wang F. et al. (2018) Co-doped Ni_3S_2@CNT arrays anchored on graphite foam with a hierarchical conductive network for high-performance supercapacitors and hydrogen evolution electrodes

Wang H et al (2011) Supercapacitive properties of hydrothermally synthesized Co3O4 nanostructures. J Phys Chem C 115(35):17599–17605

Wang Y et al (2017) A reduced graphene oxide/mixed-valence manganese oxide composite electrode for tailorable and surface mountable supercapacitors with high capacitance and super-long life. Energy Environ Sci 10(4):941–949

Wu X et al (2017) A flexible asymmetric fibered-supercapacitor based on unique Co_3O_4@ PPy core-shell nanorod arrays electrode. Chem Eng J 327:193–201

Xiao A et al (2014) Controllable synthesis of mesoporous Co_3O_4 nanoflake array and its application for supercapacitor. Mater Res Bull 60:674–678

Xu J et al (2010) Preparation and electrochemical capacitance of cobalt oxide (Co_3O_4) nanotubes as supercapacitor material. Electrochim Acta 56(2):732–736

Zhang D, Zou W (2013) Decorating reduced graphene oxide with Co_3O_4 hollow spheres and their application in supercapacitor materials. Curr Appl Phys 13(8):1796–1800

Zhang F et al (2012) Facile growth of mesoporous Co_3O_4 nanowire arrays on Ni foam for high performance electrochemical capacitors. J Power Sources 203:250–256

Zhao B et al (2015) Hollow SnO_2@Co_3O_4 core–shell spheres encapsulated in three-dimensional graphene foams for high performance supercapacitors and lithium-ion batteries. J Power Sources 298:83–91

Zhou Y et al (2018) Controlled synthesis and characterization of hybrid Sn-doped Co_3O_4 nanowires for supercapacitors. Mater Lett 216:248–251

Zhu L et al (2018) Lower ammoniation activation energy of CoN nanosheets by Mn doping with superior energy storage performance for secondary ion batteries. Nanoscale 10(12):5581–5590

Zuo W et al (2017) A novel phase-transformation activation process toward Ni–Mn–O nanoprism arrays for 24 V ultrahigh-voltage aqueous supercapacitors. Adv Materials. 29(36):1703463